

Manipulation of the Dzyaloshinskii–Moriya Interaction in Co/Pt Multilayers with Strain

N. S. Gusev,¹ A. V. Sadovnikov^{1b,2,5} S. A. Nikitov,^{2,5} M. V. Sapozhnikov^{1b,1,3} and O. G. Udalov^{1b,1,3,4}

¹*Institute for Physics of Microstructures RAS, Nizhny Novgorod 603950, Russia*

²*Saratov State University, Saratov 410012, Russia*

³*Lobachevsky State University of Nizhny Novgorod, 603950 Nizhny Novgorod, Russia*

⁴*Department of Physics and Astronomy, California State University Northridge, Northridge, California 91330, USA*

⁵*Kotelnikov Institute of Radioengineering and Electronics RAS, Moscow, 125009, Russia*

 (Received 5 August 2019; revised manuscript received 9 January 2020; accepted 20 March 2020; published 15 April 2020)

Interfacial Dzyaloshinskii–Moriya interaction (DMI) is experimentally investigated in Pt/Co/Pt multilayer films under strain. A strong variation (from 0.1 to 0.8 mJ/m²) of the DMI constant is demonstrated at $\pm 0.1\%$ in-plane uniaxial deformation of the films. The anisotropic strain induces strong DMI anisotropy. The DMI constant perpendicular to the strain direction changes sign, while the constant along the strain direction does not. Estimates show that the DMI can be controlled with an electric field in hybrid ferroelectric-ferromagnetic systems. So, the observed effect opens the way to control the DMI and eventually skyrmions with a voltage via a strain-mediated magnetoelectric coupling.

DOI: [10.1103/PhysRevLett.124.157202](https://doi.org/10.1103/PhysRevLett.124.157202)

Skyrmions in magnetic thin films with perpendicular anisotropy are nontrivial magnetic textures [1] promising various applications such as memory and logics. Therefore, manipulating (creating, annihilating, and moving) the skyrmions is an urgent but still challenging quest of modern spintronics [2–5]. So far, several approaches have been used. Electrical-current-based techniques utilizing spin torque [6–8] and spin-orbit torque [9,10] allow one to control the skyrmions but require a high current density and, therefore, have low energy efficiency. A lot of groups work on electric-field-based approaches where the heat losses are minimized. One of the most actively studied approaches is based on voltage controlled magnetic anisotropy [11–15]. Since a skyrmion stability is defined by the competition of the magnetic anisotropy and the Dzyaloshinskii–Moriya interaction (DMI), tuning of one of these contributions opens the way to control the skyrmions. So far, the field was focused on the variation of the magnetic anisotropy via a strain-mediated magnetoelectric coupling [16] or a charge-mediated magnetoelectric effect [17].

In the present Letter, we experimentally demonstrate that the DMI can be also controlled with a strain. Strain dependence of the DMI was previously studied in bulk crystals [18–20]. Here, we show that in heavy metal-ferromagnet (Co/Pt) multilayer structures the interfacial DMI coefficient can be tuned in a wide range by applying strain. The uniaxial strain modifies the average DMI constant and also introduces anisotropy to the DMI. Moreover, the DMI of different signs for different directions appears due to the uniaxial strain.

Strains in magnetic films can be induced mechanically (via bending for example) or with an electric field in hybrid ferromagnetic-ferroelectric (FM-FE) systems [21]. In our

Letter, we use mechanical means to create the strain. At that, the magnitude of deformations achieved in our experiment can be easily induced by an electric field in a ferroelectric (such as PMN-PT). This opens the way to control the DMI (and therefore skyrmions) in heavy metal (HM)-FM systems with voltage.

Note that voltage-based tuning of the DMI due to a charge accumulation was demonstrated in Pt/Co/TaO multilayers in Ref. [22]. The DMI in this system appears at the insulator-FM boundary rather than at the HM-FM interface. Therefore, the DMI in this system is much weaker (on order of 0.1 mJ/m²) than in HM-FM multilayers (on order of 1 mJ/m²). This restricts the use of insulator-FM systems in skyrmionics. Voltage-induced variation of the DMI due to the charge accumulation is challenging in HM-FM multilayers since the electric field is screened in a very thin interfacial layer. In contrast, the strain-based approach proposed in the present Letter can be applied to metallic systems, giving a promising opportunity to control skyrmions.

In the present Letter, a series of samples glass/Ta(2.5 nm)/Pt(d_{Pt})/Co(1.2 nm)/Pt(2 nm) were fabricated using dc magnetron sputtering. The thickness of the bottom Pt layer (d_{Pt}) varies from 0.4 to 2.2 nm. Fabricating samples with different Pt thickness allows us to identify the range of growth parameters with the highest susceptibility to strain. In our samples, the Co film is surrounded by two Pt layers. One can expect that the DMI cancels in this case. However, it is well known that nonzero DMI is observed in such symmetric Pt/Co/Pt systems [23]. This is because Pt/Co and Co/Pt interfaces are, in fact, not identical, since the bottom Pt layer grows on the Ta buffer, while the upper Pt layer grows on Co. Moreover, the DMI strongly depends on Pt thickness [24], which also makes the contributions of the upper and bottom interfaces different.

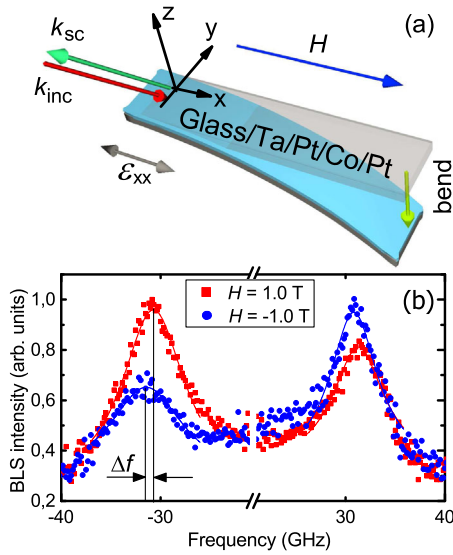


FIG. 1. (a) Experimental geometry. The sample (glass/Ta/Pt/Co/Pt) is bent and has in-plane strain ϵ_{xx} . BLS experiments are performed in the Damon-Eshbach geometry. The laser beam with the incident wave vector \mathbf{k}_{inc} (red arrow) laying in the (y,z) plane irradiates the sample. The multilayer film scatters the light back into the direction $\mathbf{k}_{\text{sc}} = -\mathbf{k}_{\text{inc}}$ (green arrow). A magnetic field H is applied perpendicular to the incidence plane. (b) Typical BLS spectrum of glass/Ta/Pt/Co/Pt without a strain at $H = 1$ T (squares) and $H = -1$ T (circles). Solid lines are Lorentzian fits. Δf is the frequency shift between the Stokes and anti-Stokes peaks.

Magnetic hysteresis loops of the samples were measured at different in-plane uniaxial strain using a magneto-optical Kerr effect (MOKE) in polar geometry. A sample was placed inside the specially designed holder [see Fig. 1(a)]. One edge of the sample was fixed in the holder, the opposite edge was bent by a screw inducing a uniaxial strain. The strain is elastic and does not produce damage to the samples (see Supplemental Material [25]). The shift of the sample's free edge caused a strain of the magnetic film in the vicinity of the fixed side, where the laser beam irradiates the film. Introducing the x axis connecting fixed and free edges [Fig. 1(a)], one can estimate the x component of the strain as $\epsilon_{xx} = 3d\Delta z/(2L^2)$ [26], where d and L are the thickness and length of the sample (glass plate), respectively, and Δz is the shift of the plate's free end. The in-plane deformation was also checked using a strain gauge.

Figure 2 shows the magnetization curves of the Co/Pt samples for different d_{Pt} . Each panel in Fig. 2 demonstrates several hysteresis loops corresponding to a different strain amplitude ϵ_{xx} . Figure 2(a) shows the case of small Pt thickness, in which the structure has an in-plane anisotropy and is not sensitive to the applied strain. The sample with a thick Pt layer [Fig. 2(b)] has a rectangular magnetization curve and no magnetostriction. The strain influences the properties of the film only when the Pt layer is close to the critical thickness at which the transition between in- and

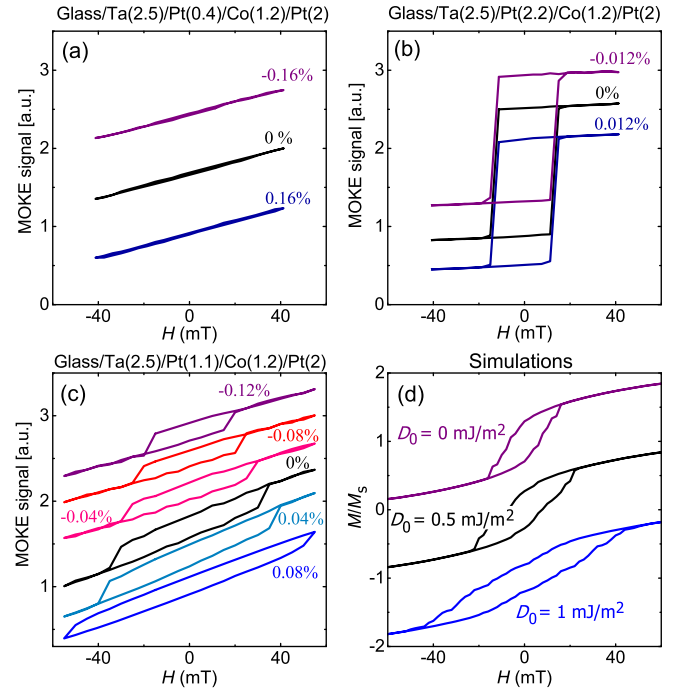


FIG. 2. Out-of-plane hysteresis loops for different strain ϵ_{xx} (shown nearby each curve) applied to the samples glass/Ta(2)/Pt(d_{Pt})/Co(1.2)/Pt(2). (a) $d_{\text{Pt}} = 0.4$, (b) $d_{\text{Pt}} = 1.1$, (c) $d_{\text{Pt}} = 2.2$ nm. (d) Micromagnetic simulation results for Co/Pt films. (a),(b) Shows magnetization hysteresis loops for films with the different DMI: $D_0 = 0$, $D_0 = 0.5$, and $D_0 = 1$ mJ/m². The corresponding values of the hysteresis widths are 34, 44, and 86 mT. The loops are shifted with respect to each other for clarity.

out-of-plane anisotropy occurs. This case is shown in Fig. 2(c). The curves in this plot consist of a linear slope and a hysteresis loop. The black line in Fig. 2(c) represents the unstrained film. Compressive strain increases the hysteresis loop width, while tensile strain reduces it. Two additional samples were also studied with the thickness of the Pt layer in the range between 1.1 and 2 nm. They have a hysteresis loop similar to the sample with $d_{\text{Pt}} = 1.1$ nm. They also demonstrate the dependence of the hysteresis loop on the strain.

The DMI in the samples was studied by Brillouin light scattering (BLS) in the Damon-Eshbach geometry [27] under application of strain in a similar way as described in the previous section [see Fig. 1(a)]. A magnetic field was applied either along the deformation direction or perpendicular to it, allowing us to measure the DMI constants along the x (D_x) and y (D_y) directions. A typical BLS spectrum is presented in Fig. 1(b). Solid lines show the Lorentzian fit, demonstrating the shift of the Stokes and anti-Stokes peaks denoted as Δf .

Following the standard approach (see Supplemental Material [25]), we estimate the DMI constant as [27,28]

$$D_i = 2M_s\Delta f/(\pi\gamma k_i), \quad (1)$$

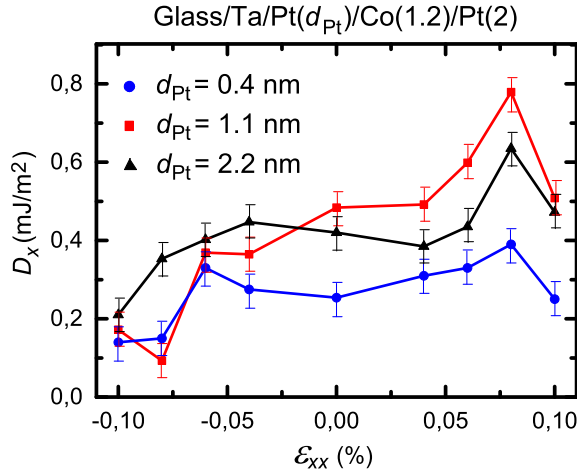


FIG. 3. The DMI constant measured along the x direction (D_x) as a function of applied strain (ϵ_{xx}). The origin of the error bars are the BLS instrument frequency uncertainty and the uncertainty occurring in the least-square fit of $\Delta f(k)$ dependencies (see details in the Supplemental Material [25]). The linear fit of the $D_x(\epsilon_{xx})$ obtained using the least-square method is provided in the Supplemental Material [25].

where M_s is the saturation magnetization, Δf is the difference between the Stokes and anti-Stokes frequencies, k_i is the momentum along the i direction (in our case $i = x$ or y), and $\gamma = 176$ GHz/T is the gyromagnetic ratio. The value of M_s used in our estimates is 1.1×10^6 A/m, which is typical for Co/Pt films [29,30].

The DMI constant along the x direction for the three samples with the Pt thickness varying from 0.4 to 2.2 nm is shown in Fig. 3 as a function of strain ϵ_{xx} . Two samples with $d_{\text{Pt}} = 1.1$ and 2.2 nm demonstrate a strong enough experimentally noticeable change of the DMI constant D_x with strain. For the sample with $d_{\text{Pt}} = 0.4$ nm, the variations of the DMI is weaker.

The microscopic reason for the DMI strain dependence can be understood using the theoretical model by Fert and Levy [31]. According to this model, the DMI is mediated by conducting electrons hopping between magnetic ions through heavy metal ions. Since the interaction appears due to the conduction electrons, it has oscillating character and is described by the expression

$$W_{\text{DMI}} \sim \sin[k_F(a + 2b) + \pi Z_d/10] \sin(2\theta)/(ab^2), \quad (2)$$

where k_F is the Fermi momentum, a is the distance between magnetic (Co) ions (see Fig. 4), b is the distance between magnetic and heavy metal (Pt) ions, Z_d is the number of d electrons, and θ is the angle made by vectors connecting the heavy metal ion and two magnetic ions.

The in-plane strain produced by bending changes the distances a and b . For example, the tensile strain along the x axis increases a but decreases the height of Pt ion (see left panel in Fig. 4). The height reduces according to Poisson law. This modifies the DMI constant. Equation (2) gives

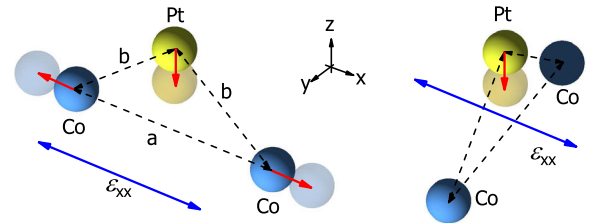


FIG. 4. Displacement of Co and Pt ions due to xx tensile strain ϵ_{xx} . a is the distance between the Co ions. b is the distance between the Pt and Co ions. (Left) The ion triangle oriented along the x axis. (Right) The triangle oriented perpendicular to the strain axis.

nonmonotonic behavior of the DMI constant as a function of distances. This probably is the reason for the non-monotonic behavior of the DMI constant at a high strain.

Note, however, that the proposed consideration does not explain the dependence of the DMI strain variation on the Pt layer thickness. First, the model includes only one neighboring Pt layer, while all other layers may contribute. Another factor is that d_{Pt} influences the lattice constant a in the Pt layer closest to the Co film.

Since the strain induced in our samples is anisotropic, one can expect that the DMI is also anisotropic. This is demonstrated in Fig. 5, where the behavior of the DMI coefficient for two different directions is shown for the sample with $d_{\text{Pt}} = 1.1$ nm. The uniaxial deformation changes the DMI coefficient for both directions. For tensile strain $D_x \approx D_y$, but for compressive strain there is a strong anisotropy of the DMI coefficient $D_x \neq D_y$.

The DMI anisotropy can be also understood using Eq. (2). When the deformation is applied along the x axis, the DMI constant along this direction is modified due to

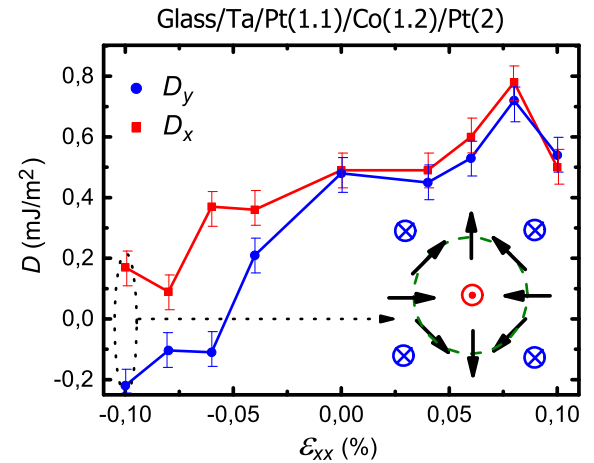


FIG. 5. The DMI constant measured along the x and y directions ($D_{x,y}$) as a function of applied strain (ϵ_{xx}) for the sample with $d_{\text{Pt}} = 1.1$ nm. See the linear least-square fits in the Supplemental Material [25]. (Inset) The skyrmion with an antivortex domain wall. It may appear due to the anisotropic DMI with a different sign along different directions [32].

variation of both a and b (see left panel in Fig. 4). At that, the DMI constant in the y direction is defined by ion triangles along the y axis. These triangles are modified in a different way (see right panel in Fig. 4). The distance between magnetic ions a is not changed, while the height of the Pt ion reduces. So, variation of the DMI constant in this direction is different.

What is even more interesting is that at strong compressive strain the y component of the DMI changes the sign, while the x component does not. In Ref. [32] the authors simulate magnetic skyrmions in the situation with different signs of the DMI along different directions. They show that the skyrmion with an antivortex domain wall (see inset in Fig. 5) can be realized in this case. So, the strained Co/Pt films can be a good candidates for studying such “antivortex” skyrmions.

Usually, the interface-induced DMI in the thin film is described by the expression $-D(\mathbf{m} \cdot [[\mathbf{z} \times \nabla] \times \mathbf{m}])$, where D is the DMI constant, \mathbf{m} is the normalized magnetization vector, and \mathbf{z} is the interface normal. This expression describes the system isotropic in the film plane. In our Letter, we use uniaxial strain inducing the anisotropic DMI. The interaction energy W_{DMI} can be described by the expression

$$W_{\text{DMI}} = D_x \left(m_x \frac{\partial m_z}{\partial x} - m_z \frac{\partial m_x}{\partial x} \right) + D_y \left(m_y \frac{\partial m_z}{\partial y} - m_z \frac{\partial m_y}{\partial y} \right). \quad (3)$$

In the linear approximation, the constants $D_{x,y}$ can be expressed via strain as follows:

$$D_{x,y} = D_{0x,y} + D_1(\epsilon_{xx} + \epsilon_{yy}) \pm D_{\text{an}}(\epsilon_{xx} - \epsilon_{yy}), \quad (4)$$

where the tensor ϵ is the strain in the film, the sign “+” (“−”) is for D_x (D_y). The first term describes the anisotropic DMI in the unstrained film, the second term shows the influence of the isotropic strain, and the third contribution represents the effect of the anisotropic deformation.

Using a linear least-squares fit (see Supplemental Material [25]) of our data, we get the constants D_{0x} , D_1 , and D_{an} for our samples. The obtained results are summarized in Table I. The first three lines are for samples shown in Fig. 3. The two bottom lines are for two additional samples mentioned above. The second column indicates the anisotropy (Anis.) type in each sample. Two additional samples studied here have the “mixed” type of magnetic hysteresis loop similar to the sample with $d_{\text{Pt}} = 1.1$ nm. While the uncertainty of the data is significant, all the samples have nonzero sensitivity to strain (see $D_1 + D_{\text{an}}$). The samples with the mixed anisotropy type ($d_{\text{Pt}} = 1.1$ and $d_{\text{Pt}} = 1.9$ nm) have the highest average sensitivity. The mixed type of the anisotropy and high average $D_1 + D_{\text{an}}$ appear in the samples with intermediate Pt thickness. The samples with thin small ($d_{\text{Pt}} = 0.4$ nm) and high ($d_{\text{Pt}} = 2.2$ nm) Pt thickness have lower strain sensitivity.

TABLE I. DMI constants for different samples. The first three lines show the data for the sample in Figs. 3 and 5. The last two lines show the data for two additional samples. The constants D_{0x} and D_{0y} are measured in mJ/m^2 , D_1 and D_{an} are measured in $\text{mJ}/[\text{m}^2(\%)]$. The samples’ thickness is defined with the precision of 20%.

d_{Pt} , nm	Anis.	D_{0x}	D_{0y}	D_1	D_{an}	$D_1 + D_{\text{an}}$
0.4	In plane	0.27 ± 0.03	0.7 ± 0.6
1.1	Mixed	0.43 ± 0.08	0.3 ± 0.1	3.4 ± 1.1	-0.9 ± 0.6	2.5 ± 1.1
1.9	Mixed	0.4 ± 0.05	0.2 ± 0.1	3.2 ± 0.7	-1 ± 0.8	2.5 ± 1.4
2	Mixed	0.42 ± 0.02	0.4 ± 0.03	2.1 ± 1	-0.5 ± 0.3	1.6 ± 0.8
2.2	Perp.	0.42 ± 0.03	1.1 ± 0.8

The films with the mixed anisotropy type demonstrate strong DMI anisotropy also (see D_{an}).

The strain induced in our films due to the bending of the samples is on the order of 0.1%. Such a value can be easily achieved in ferroelectric crystals under application of voltage. For example, in $\text{Pb}(\text{Mg}_{1/3}\text{Nb}_{2/3})\text{O}_3\text{PbTiO}_3$ (PMN-PT) crystal, the voltage-induced strain reaches 0.3% [33], which is even higher than what we use in our experiments. So, one can control DMI with voltage in ferroelectric-(Co/Pt) systems. Assuming linear dependence of the DMI coefficient on ϵ , one can expect modulation of the DMI constant from -0.8 to 1.8 mJ/m^2 in the electric field range of about ± 600 V/mm in the PMN-PT/Ta/Pt/Co/Pt system. Note that for certain cuts of the PMN-PT crystal the induced strain is highly anisotropic. So, the voltage controlled DMI anisotropy can also be realized.

Using micromagnetic simulations (the OOMMF code [34]), we demonstrate that the strain-induced change of the magnetization hysteresis loop shown in Fig. 2(c) can be explained by the strain-induced DMI variation. The results of the micromagnetic simulations are shown in Fig. 2(d). In the simulations, we assumed the isotropic DMI varying with the strain similar to what we observed in our BLS experiments ($D_0 = 0, 0.5, \text{ and } 1$ mJ/m^2). The saturation magnetization $M_s = 1.1 \times 10^6$ A/m and the exchange stiffness $A = 2 \times 10^{11}$ J/m [30] were uniform across the film. The magnitude of the perpendicular (Perp.) uniaxial anisotropy varies across the sample between $K_{\text{min}} = 6.3 \times 10^5$ and $K_{\text{max}} = 8.3 \times 10^5$ J/m³. These values are near the critical anisotropy $K = \mu_0 M_s^2 / 2 = 7.6 \times 10^5$ J/m³ corresponding to the easy-plane–easy-axis transition. The parameters used are in agreement with what we obtained from fitting of BLS data. The BLS data confirm also that the anisotropy varies weakly with strain (see Supplemental Material [25]).

Increasing the DMI reduces the domain wall energy and increases the magnetic field at which domains disappear

(the hysteresis loop width). This is in agreement with our experimental observations (Fig. 2). So, we conclude that the magnetization loop variations observed for the film with the intermediate anisotropy are in good agreement with our BLS data.

In summary, we performed BLS and MOKE studies of strained Pt/Co/Pt films. We demonstrated that the strain strongly influences the DMI in the system. Moreover, strong DMI anisotropy appears under compressive strain. The DMI constant perpendicular to the strain direction changes sign, while the constant along the strain direction does not. The strain used in the present Letter is less than what can be achieved in a hybrid FE-FM system. This opens the way to manipulate the DMI and eventually the skyrmions with a voltage via the strain-mediated magnetoelectric coupling.

Sample fabrication, MOKE measurements and numerical modeling were supported by the Russian Science Foundation (Grant No. 18-72-10026). BLS measurements were supported by the Russian Foundation for Basic Research (Projects No. 18-29-27026, No. 18-57-76001), Russian Science Foundation (Grant No. 16-19-10283), and Grant of the President of Russian Federation (MK-1870.2020.9, SP-2819.2018.5). We thank I. S. Beloborodov for fruitful discussions.

-
- [1] N. Nagaosa and Y. Tokura, *Nat. Nanotechnol.* **8**, 899 (2013).
 [2] A. Fert, N. Reyren, and V. Cros, *Nat. Rev. Mater.* **2**, 17031 (2017).
 [3] K. Everschor-Sitte, J. Masell, R. M. Reeve, and M. Klui, *J. Appl. Phys.* **124**, 240901 (2018).
 [4] G. Finocchio, F. Bttner, R. Tomasello, M. Carpentieri, and M. Klui, *J. Phys. D* **49**, 423001 (2016).
 [5] A. Soumyanarayanan, M. Raju, A. L. Gonzalez Oyarce, A. K. C. Tan, M.-Y. Im, A. P. Petrovic, P. Ho, K. H. Khoo, M. Tran, C. K. Gan, F. Ernult, and C. Panagopoulos, *Nat. Mater.* **16**, 898 (2017).
 [6] W. Jiang, P. Upadhyaya, W. Zhang, G. Yu, M. B. Jungfleisch, F. Y. Fradin, J. E. Pearson, Y. Tserkovnyak, K. L. Wang, O. Heinonen, S. G. E. te Velthuis, and A. Hoffmann, *Science* **349**, 283 (2015).
 [7] A. Hrabec, J. Sampaio, M. Belmeguenai, I. Gross, R. Weil, S. M. Chrif, A. Stashkevich, V. Jacques, A. Thiaville, and S. Rohart, *Nat. Commun.* **8**, 15765 (2017).
 [8] J. Sampaio, V. Cros, S. Rohart, A. Thiaville, and A. Fert, *Nat. Nanotechnol.* **8**, 839 (2013).
 [9] G. Yu, P. Upadhyaya, X. Li, W. Li, S. K. Kim, Y. Fan, K. L. Wong, Y. Tserkovnyak, P. K. Amiri, and K. L. Wang, *Nano Lett.* **16**, 1981 (2016).
 [10] F. Bttner, I. Lemesch, M. Schneider, B. Pfau, C. M. Gnther, P. Hensing, J. Geilhufe, L. Caretta, D. Engel, B. Krger, J. Viehhaus, S. Eisebitt, and G. S. D. Beach, *Nat. Nanotechnol.* **12**, 1040 (2017).
 [11] L. Wang, Q. Feng, Y. Kim, R. Kim, K. H. Lee, S. D. Pollard, Y. J. Shin, H. Zhou, W. Peng, D. Lee, W. Meng, H. Yang, J. H. Han, M. Kim, Q. Lu, and T. W. Noh, *Nat. Mater.* **17**, 1087 (2018).
 [12] Y. Liu, N. Lei, W. Zhao, W. Liu, A. Ruotolo, H.-B. Braun, and Y. Zhou, *Appl. Phys. Lett.* **111**, 022406 (2017).
 [13] J. Wang, Y. Shi, and M. Kamlah, *Phys. Rev. B* **97**, 024429 (2018).
 [14] A. V. Sadovnikov, A. A. Grachev, S. E. Sheshukova, Y. P. Sharaevskii, A. A. Serdobintsev, D. M. Mitin, and S. A. Nikitov, *Phys. Rev. Lett.* **120**, 257203 (2018).
 [15] Y. Shi and J. Wang, *Phys. Rev. B* **97**, 224428 (2018).
 [16] Y. Sun, Y. Ba, A. Chen, W. He, W. Wang, X. Zheng, L. Zou, Y. Zhang, Q. Yang, L. Yan, C. Feng, Q. Zhang, J. Cai, W. Wu, M. Liu, L. Gu, Z. Cheng, C.-W. Nan, Z. Qiu, Y. Wu, J. Li, and Y. Zhao, *ACS Appl. Mater. Interfaces* **9**, 10855 (2017).
 [17] B. Dieny and M. Chshiev, *Rev. Mod. Phys.* **89**, 025008 (2017).
 [18] Y. Nii, T. Nakajima, A. Kikkawa, Y. Yamasaki, K. Ohishi, J. Suzuki, Y. Taguchi, T. Arima, Y. Tokura, and Y. Iwasa, *Nat. Commun.* **6**, 8539 (2015).
 [19] K. Shibata, J. Iwasaki, N. Kanazawa, S. Aizawa, T. Tanigaki, M. Shirai, T. Nakajima, M. Kubota, M. Kawasaki, H. S. Park, D. Shindo, N. Nagaosa, and Y. Tokura, *Nat. Nanotechnol.* **10**, 589 (2015).
 [20] T. Koretsune, N. Nagaosa, and R. Arita, *Sci. Rep.* **5**, 13302 (2015).
 [21] S. Geprgs, A. Brandlmaier, M. Opel, R. Gross, and S. T. B. Goennenwein, *Appl. Phys. Lett.* **96**, 142509 (2010).
 [22] C. Baraduc, T. Srivastava, M. Schott, M. Belmeguenai, Y. Roussign, A. Bernand-Mantel, L. Ranno, S. Pizzini, S. M. Chrif, A. Stashkevich, S. Auffret, M. Chshiev, and H. Ba, *Proc. Spintron. XI* **10732**, 1073232 (2018).
 [23] A. V. Davydenko, A. G. Kozlov, A. G. Kolesnikov, M. E. Steblyi, G. S. Suslin, Y. E. Vekovshinin, A. V. Sadovnikov, and S. A. Nikitov, *Phys. Rev. B* **99**, 014433 (2019).
 [24] S. Tacchi, R. E. Troncoso, M. Ahlberg, G. Gubbiotti, M. Madami, J. Åkerman, and P. Landeros, *Phys. Rev. Lett.* **118**, 147201 (2017).
 [25] See Supplemental Material at <http://link.aps.org/supplemental/10.1103/PhysRevLett.124.157202> which provides information on the measurements procedures and fitting procedures. There is also data for two additional samples mentioned in the main text.
 [26] L. Landau and E. Lifshitz, *Theory of Elasticity*, A Course of Theoretical Physics Vol. 7 (Pergamon Press, New York, 1970).
 [27] K. Di, V. L. Zhang, H. S. Lim, S. C. Ng, M. H. Kuok, J. Yu, J. Yoon, X. Qiu, and H. Yang, *Phys. Rev. Lett.* **114**, 047201 (2015).
 [28] J.-H. Moon, S.-M. Seo, K.-J. Lee, K.-W. Kim, J. Ryu, H.-W. Lee, R. D. McMichael, and M. D. Stiles, *Phys. Rev. B* **88**, 184404 (2013).
 [29] L. Sun, R. X. Cao, B. F. Miao, Z. Feng, B. You, D. Wu, W. Zhang, A. Hu, and H. F. Ding, *Phys. Rev. Lett.* **110**, 167201 (2013).
 [30] C. Eyrych, W. Huttema, M. Arora, E. Montoya, F. Rashidi, C. Burrowes, B. Kardasz, E. Girt, B. Heinrich, O. N. Mryasov, M. From, and O. Karis, *J. Appl. Phys.* **111**, 07C919 (2012).
 [31] A. Fert and P. M. Levy, *Phys. Rev. Lett.* **44**, 1538 (1980).

- [32] L. Camosi, S. Rohart, O. Fruchart, S. Pizzini, M. Belmeguenai, Y. Roussigne, A. Stashkevich, S. M. Cherif, L. Ranno, M. de Santis, and J. Vogel, *Phys. Rev. B* **95**, 214422 (2017).
- [33] H. Sohn, M. E. Nowakowski, C. y. Liang, J. L. Hockel, K. Wetzlar, S. Keller, B. M. McLellan, M. A. Marcus, A. Doran, A. Young, M. Klui, G. P. Carman, J. Bokor, and R. N. Candler, *ASC Nano* **9**, 4814 (2015).
- [34] M. Donahue and D. Porter, *OOMMF User's Guide Version 1.0* (National Institute of Standards and Technology, Gaithersburg, MD, 1999).